QUARTERLY JOURNAL OF THE ROYAL METEOROLOGICAL SOCIETY
Q. J. R. Meteorol. Soc. (2009)
Published online in Wiley InterScience
(www.interscience.wiley.com) DOI: 10.1002/qj.403

An evaluation of the long-wave radiative transfer code used in the Met Office Unified Model

C. Goldblatt,[a,b]* T. M. Lenton[a] and A. J. Watson[a]
[a]*School of Environmental Sciences, University of East Anglia, UK*
[b]*Space Science and Astrobiology Division, NASA Ames Research Center, USA*

ABSTRACT: A detailed evaluation of the radiative transfer code used in the Met Office Unified Climate/Forecast Model is performed, comparing it with a line-by-line model and testing the climatic effects of errors in a radiative–convective model. The radiative forcing at the tropopause due to CO_2 changes within SRES scenarios and across Quaternary glacial cycles is represented with reasonable accuracy, suggesting that surface temperature will be correctly predicted. However, this is achieved by partial cancellation of opposing errors in upward and downward fluxes. The changes in the vertical profiles of radiative fluxes and the changes to surface and top-of-atmosphere fluxes all show significant errors, even at twice pre-industrial CO_2. This causes a sign error in the change in the convective flux in the radiative–convective model. Performance of the code deteriorates rapidly above four times pre-industrial CO_2. For less-abundant greenhouse gases, CH_4 and N_2O, the errors are larger as a proportion of their radiative forcings. Errors for surface and top-of-atmosphere fluxes for CO_2 are similar to those from the mean of the general circulation model (GCM) codes submitted to the intercomparison of radiation codes for IPCC AR4, implying that errors as found here may not be uncommon in climate models. A renewed emphasis on accuracy in radiative transfer calculations and openness in intercomparison studies is necessary to improve the modelling of climate change.

KEY WORDS climate model; radiative forcing; GCM; carbon dioxide; methane; nitrous oxide; WMGHG; greenhouse gas

Received 6 June 2008; Revised 30 January 2009; Accepted 11 February 2009

1. Introduction

Predicting the climatic response to increasing concentration of carbon dioxide and other greenhouse gases is a major component of contemporary meteorological research. The most fundamental part of this problem is the representation of the radiative transfer in general circulation models (GCMs) and other climate models. Accuracy of the codes used for radiative transfer is therefore critical to the entire modelling effort.

Recently, Collins *et al.* (2006) performed an intercomparison of radiative forcings used in climate models for the Intergovernmental Panel on Climate Change (IPCC) Fourth Assessment Report (AR4). They found that benchmark line-by-line calculations were in excellent agreement, but that there were substantial discrepancies amongst the codes used in GCMs. Whilst this study represents an excellent starting point for intercomparisons of GCM codes, it was limited in two important respects. The first was by the small range of gas concentrations; the maximum change in CO_2 concentration considered was doubling from pre-industrial levels (287 ppmv to 574 ppmv) and the maximum change for other greenhouse gases was from pre-industrial to year 2000 concentrations (806 ppbv to 1760 ppbv for CH_4 and 275 ppbv to 316 ppbv for N_2O). The IPCC Special Report on Emissions Scenarios (SRES, Nakićenović *et al.*, 2000) suggests year 2100 abundances of up to 1248 ppmv for CO_2, 3731 ppbv for CH_4 and 460 ppbv for N_2O. Considering millennial timescale (Lenton, 2006; Lenton *et al.*, 2006) and palaeoclimate (e.g. Bergman *et al.*, 2004; Kiehl and Dickinson, 1987) requires wider ranges of concentrations still. The second was that unlike previous intercomparisons (e.g. Ellingson *et al.*, 1991), Collins *et al.* (2006) were not able to ascribe results to individual climate models, so that their study is not of use in understanding the behaviour of any specific model.

In this article, we conduct a detailed evaluation of the performance of the radiative transfer code that is used in the Met Office Unified Climate/Forecast Model (UM). In section 3, we conduct an intercomparison similar to the IPCC AR4 intercomparison (Collins *et al.*, 2006), extended by considering a much wider range of gas concentrations, considering upward and downward fluxes separately, and using a more sensitive set of metrics for intercomparison. In section 4, we look at the profiles of radiative fluxes and heating rate with height. In section 5, we use a simple radiative convective model to evaluate the climatic influences of errors in the radiative transfer codes.

2. Model descriptions

Radiative transfer is a wavelength-dependent process; absorption of radiation occurs at certain wavelengths

*Correspondence to: C. Goldblatt, Space, Science and Astrobiology Division, NASA Ames Research Center, MS 245-3, Moffett Field, CA 94035, USA.
E-mail: colin.goldblatt@nasa.gov

according to the vibration–rotation spectra of the constituent atmospheric gases (Goody and Yung, 1989). Two main types of radiative transfer code exist to solve this problem: line-by-line (LBL) codes and band models. The former type resolve all known absorption lines, thereby providing an absolute standard for radiative transfer calculation (Goody and Yung, 1989; Clough *et al.*, 1992; Clough and Iacono, 1995; Clough *et al.*, 2005). We use the Atmosphere Environment Research Inc. (AER) line-by-line model (Clough *et al.*, 1992; Clough and Iacono, 1995; Clough *et al.*, 2005), which is available from http://rtweb.aer.com/. We use version 11.3 of the model, with the associated line file program LNFL version 2.5 (based on HITRAN 2004, Rothman *et al.*, 2005), and sum for irradiances with RADSUM version 2.4 (Clough *et al.*, 2005).

For climate modelling, band models are employed as line-by-line models are too computationally expensive. The band models used in the Met Office GCM were developed by Edwards and Slingo (1996) and modified by Cusack *et al.* (1999); they are commonly known as the 'Edwards–Slingo code' (ES). This is a flexible code, providing variable spectral resolution. Data for parametrization of radiative absorption and other processes are provided in a 'spectral file'. We include four spectral files in our intercomparison here. `sp_lw_300_orig` is the original 300 band (narrow-band) long-wave spectral file, in which absorption coefficients were derived by the exponential-sum fitting of transmissions (ESFT) technique, and is used as an internal standard for the suite of Edwards–Slingo codes (Edwards and Slingo, 1996). `sp_lw_hadcm3`, `sp_lw_hadgem1_1` and `sp_lw_hadgem1_3` are broad-band (eight-band for HadCM3, nine-band for HadGEM1), the absorption coefficients for which were derived with the correlated-*k* method (Cusack *et al.*, 1999). These are used in the HadCM3 and HadGEM1 'families' of the UM (see Pope *et al.*, 2007, for a general description of these models). The spectral information is based on HITRAN 1992 (Rothman *et al.*, 1992), except for water vapour in the HadGEM spectral files which are updated to HITRAN 2001 (Rothman *et al.* 2003; J. Edwards, personal communication, 2008). All the long-wave spectral files are for the wavelength range 3.3 to 10 000 μm. We run version `esrad100407` of the Edwards–Slingo code for clear skies using the two-stream solver with direct solution, a Lambertian surface and random overlap of gases, and include continuum absorption and Doppler broadening.

In section 5 we use a radiative–convective model in which radiative transfer is calculated with the Edwards–Slingo codes to solve for the global annual mean vertical structure of the atmosphere. Convective adjustment in the model is to the pseudoadiabatic (moist) lapse rate. We assume a fixed relative humidity profile in normalized pressure coordinates (Manabe and Wetherald, 1967) and a solar zenith angle of 60°. The model uses a Newton–Raphson method to solve for equilibrium. Our fixed-profile comparisons are for clear sky conditions. In order that our radiative–convective model corresponds to this we use a simplification introduced by Kasting *et al.* (1984) and widely employed in palaeoclimate studies: clouds are not explicitly included, but a higher surface albedo is used to represent the net effect of clouds on the surface energy budget. The albedo is tuned to give $T_s = 288$ K. A detailed description of the development, numerical method and testing of the model is given by Goldblatt (2008).

3. Fixed profile, three level comparisons

3.1. Methods

We focus on the long-wave spectral region. The set-up of atmospheric profiles follows Collins *et al.* (2006). For all runs, the same 51 layer midlatitude summer profile, including oxygen, ozone and water vapour, is used (Anderson *et al.*, 1986). This is a clear-sky (cloud-free) profile. The standard atmosphere used here corresponds to pre-industrial conditions with $f\mathrm{CO}_2 = 287$ ppmv, $f\mathrm{CH}_4 = 806$ ppbv and $f\mathrm{N}_2\mathrm{O} = 275$ ppbv (i.e. Collins *et al.*, 2006, case 3a). The mixing ratio of each gas is varied in isolation, with the remaining two kept at standard, pre-industrial, values.

For the line-by-line calculation, Collins *et al.* (2006) take the long-wave spectral region as 4–100 μm so we use this region where direct comparison with their results is made. However, as all the ES spectral files use the wider range of 3.3–10 000 μm, we use this for the bulk of the LBL runs. These correspond to wavenumber ranges of 100–2500 cm^{-1} and 1–3030 cm^{-1} respectively. The AER LBL code can be run over a maximum wavenumber range of 2000 cm^{-1}, so it is necessary to split the long-wave spectral region into two parts, to calculate irradiances separately and to sum these.

As with Collins *et al.* (2006), performance of the codes is evaluated at three levels: the top of the atmosphere (TOA), a pseudotropopause at 200 hPa and the surface. Upward and downward fluxes are considered separately. The surface is taken to be a black body, so the upward flux depends only on temperature ($F_{\mathrm{lw,surf}}\uparrow = \sigma T_*^4$) and downward flux at the TOA is zero. Neither varies with greenhouse gas concentrations, so changes in the net flux at these levels depend on one radiation stream only. At the tropopause the net flux is the sum of the two streams. The net flux is defined positive downwards,

$$F = F\downarrow - F\uparrow. \tag{1}$$

To evaluate the performance of the radiative transfer codes, a number of different metrics are employed. Taking the flux at standard (pre-industrial) conditions as F_0, a forcing can be defined:

$$\mathscr{F} = F - F_0. \tag{2}$$

This was the only metric used by Collins *et al.* (2006). This will show the response to increasing gas concentration, removing any differences in the fluxes for standard conditions. At the tropopause, this forcing is generally

DOI: 10.1002/qj

referred to as the radiative forcing. The error in forcing in the band models is calculated relative to the LBL code:

$$E_{\mathscr{F}} = \frac{\mathscr{F} - \mathscr{F}_{\mathrm{LBL}}}{\mathscr{F}_{\mathrm{LBL}}}. \quad (3)$$

Letting F_i be the flux at gas concentration X_i, the flux gradient with respect to gas mixing ratio is defined as

$$G = \frac{\mathrm{d}F}{\mathrm{d}X} \approx \frac{\Delta F}{\Delta X} = \frac{F_{i+1} - F_i}{X_{i+1} - X_i}. \quad (4)$$

This is a key quantity for evaluating the response to changing gas concentration and is independent of the standard gas concentration. Gas concentrations are incremented logarithmically, such that $X_{i+1} = 10^{0.1} X_i$. The error in the flux gradient is found to be

$$\begin{aligned} E_G &= \frac{\dfrac{\mathrm{d}F}{\mathrm{d}X} - \dfrac{\mathrm{d}F_{\mathrm{LBL}}}{\mathrm{d}X}}{\dfrac{\mathrm{d}F_{\mathrm{LBL}}}{\mathrm{d}X}} = \frac{\mathrm{d}F - \mathrm{d}F_{\mathrm{LBL}}}{\mathrm{d}F_{\mathrm{LBL}}} \\ &\approx \frac{\Delta F - \Delta F_{\mathrm{LBL}}}{\Delta F_{\mathrm{LBL}}} \\ &\approx \frac{(F_{i+1} - F_i) - (F_{\mathrm{LBL},i+1} - F_{\mathrm{LBL},i})}{F_{\mathrm{LBL},i+1} - F_{\mathrm{LBL},i}}. \end{aligned} \quad (5)$$

This provides a quantitative standard to measure the accuracy of the band models under changing gas concentrations. However, by derivation, it is insensitive to the magnitude of the flux gradient, so does not impart information about the climatic implication of the error in radiative forcing. This is most important in the case of small flux gradients; a large relative error in flux gradient will be climatically unimportant if the flux gradient itself is small (i.e. if the expected effect of increasing the greenhouse gas concentration is trivial). Thus another useful metric is the absolute error in radiative forcing due to a given change in gas concentration, taken to be a doubling in concentration. This 'doubling error' is defined as

$$\begin{aligned} D &= \left(\frac{\mathrm{d}F}{\mathrm{d}(\log X)} - \frac{\mathrm{d}F_{\mathrm{LBL}}}{\mathrm{d}(\log X)} \right) \log 2 \\ &\approx \left(\frac{\Delta F}{\Delta(\log X)} - \frac{\Delta F_{\mathrm{LBL}}}{\Delta(\log X)} \right) \log 2 \\ &\approx \left(\frac{(F_{i+1} - F_i) - (F_{\mathrm{LBL},i+1} - F_{\mathrm{LBL},i})}{\log(X_{i+1}) - \log(X_i)} \right) \log 2. \end{aligned} \quad (6)$$

3.2. Results

The fluxes at standard conditions are given in Table I. These may give an indication of the absolute accuracy of the radiative transfer code. However, factors other than the representation of gaseous absorption may affect this, for example changes in the spectral database or the method of angular integration of radiances used. The restricted spectral range used by Collins *et al.* (2006) for LBL runs is also important here, resulting in smaller fluxes. For example, for a surface of emissivity 1 and temperature 294.2 K, the full black-body flux is 424.80 W m^{-2} whereas the flux in the spectral region used by Collins *et al.* (2006) for LBL runs is 421.93 W m^{-2}. Hence using this restricted spectral range will necessarily give an underestimate of absolute fluxes. Compared with the AER LBL code for the same spectral region, errors for individual streams (excluding the upward flux at the surface, which does not depend on gaseous absorption) for the ES spectral files are 0.02–0.86 W m^{-2} for the narrow-band spectral file and 0.14–3.82 W m^{-2} for the broad-band spectral files.

The response of a GCM to increased greenhouse gas concentrations likely depends more on the change in fluxes, as it will have been tuned to give a certain temperature field at standard conditions. As a prelude to comparison across a wide range of concentrations, consider the standard case of doubling CO_2 from pre-industrial concentrations (Table II). This is done with zero concentrations of CH_4 and N_2O so that it is directly comparable to case case 2b–1a of the intercomparison of radiative forcing in climate models used for IPCC AR4 (Collins *et al.*, 2006). We also include comparison runs using the MRTA line-by-line code with spectral data from HITRAN 1992 and 2004 databases as a test of the influence of the different spectral databases used by the AER LBL code and the Edwards–Slingo code (Kratz 2008; D. Kratz, personal communication, 2008).

First, compare the three sets of LBL results (RTMIP ensemble, AER LBL, MRTA). These results are similar, though not identical. MRTA and AER LBL forcings differ from the mean of the RTMIP ensemble ($\langle \mathscr{F}_{\mathrm{RTMIPLBL}} \rangle$) by up to 0.15 W m^{-2} or 2.5 standard deviations. MRTA was included in RTMIP but AER LBL was not. Some of these differences likely arise from differences in the profiles used. Whilst these are all MLS profiles, there are unfortunately differences in the definitions used for this 'standard' profile. We follow the more recent definition by Anderson *et al.* (1986) for the AER LBL runs, whereas Kratz (2008) uses an older definition by McClatchey *et al.* (1971); there are non-trivial differences between these. Collins *et al.* (2006) cite Anderson *et al.* (1986), but use a surface temperature of 294.0 K, which is from the McClatchey *et al.* (1971) profile, rather than 294.2 K from Anderson *et al.* (1986). There are also differences in the number of levels used in the profiles: we use 52, Collins *et al.* (2006) use 259 and Kratz (2008) uses 35. For the two AER LBL runs for different spectral regions the difference in forcings from CO_2 doubling is negligible.

Now compare the Edwards–Slingo code with the AER LBL code (these results from this study are from identical profiles and spectral regions). The narrow-band spectral file agrees well with the AER LBL code, with errors of a few per cent. By contrast, the broad-band spectral files all perform poorly compared with either the AER LBL code or the narrow-band spectral file (which acts as an internal standard for the suite of Edwards–Slingo spectral files), with errors of 23.7%–41.9% at the surface, 2.3%–7.8% in individual streams at the tropopause and 10.9%–11.5% at the TOA. Errors in the net flux at the tropopause are much smaller ($< 1\%$), which if viewed alone would suggest good performance. However, this

DOI: 10.1002/qj

Table I. Fluxes at standard conditions. Spectral regions for the AER LBL model are (a) 4–100 μm, corresponding to Collins *et al.* (2006), and (b) 3.3–10 000 μm, corresponding to the ES spectral range.

		Surface			200 hPa			TOA
Code (Spectral region)	Performance metric	$F\downarrow$	F	$F\uparrow$	$F\downarrow$	F	$F\uparrow$	$F\uparrow$
AER LBL (a)	$F_{\mathrm{LBLa},0}$ (W m^{-2})	345.50	−76.43	421.93	23.65	−263.83	287.47	280.61
AER LBL (b)	$F_{\mathrm{LBLb},0}$ (W m^{-2})	347.74	−76.96	424.70	24.41	−265.19	289.60	282.72
ES `sp_lw_300_orig`	F_0 (W m^{-2})	346.88	−77.80	424.68	23.67	−265.58	289.25	282.69
	$F_0 - F_{\mathrm{LBLb},0}$ (W m^{-2})	−0.86	−0.84	−0.01	−0.74	−0.40	−0.35	−0.02
ES `sp_lw_hadcm3`	F_0 (W m^{-2})	348.62	−76.06	424.68	22.86	−263.40	286.26	279.58
	$F_0 - F_{\mathrm{LBLb},0}$ (W m^{-2})	0.88	0.90	−0.01	−1.55	1.79	−3.34	−3.14
ES `sp_lw_hadgem1_1`	F_0 (W m^{-2})	349.01	−75.67	424.68	22.78	−262.99	285.77	279.09
	$F_0 - F_{\mathrm{LBLb},0}$ (W m^{-2})	1.27	1.29	−0.01	−1.63	2.20	−3.82	−3.63
ES `sp_lw_hadgem1_3`	F_0 (W m^{-2})	347.60	−77.08	424.68	22.88	−267.05	289.94	283.27
	$F_0 - F_{\mathrm{LBLb},0}$ (W m^{-2})	−0.14	−0.13	−0.01	−1.52	−1.87	0.34	0.55

Table II. Radiative forcing error for CO_2 doubling. CO_2 is increased from 287 to 574 ppmv with no CH_4 or N_2O, corresponding to RTMIP (Collins *et al.*, 2006) case 2b-1a. RTMIP data are from Collins *et al.* (2006), Table 8. MRTA data were supplied by D. Kratz (personal communication, 2008) following Kratz (2008). AER LBL and ES data are from this study. Spectral regions for the AER LBL model are (a) 4–100 μm, corresponding to Collins *et al.* (2006), and (b) 3.3–10 000 μm, corresponding to the ES spectral range.

		Surface		200 hPa		TOA
Code	Performance metric	$F\downarrow$	$F\downarrow$	F	$F\uparrow$	$F\uparrow$
RTMIP LBL	$\langle\mathscr{F}_{\mathrm{RTMIP\,LBL}}\rangle$, σ (W m^{-2})	1.64, 0.04	–	5.48, 0.07	–	−2.80, 0.06
RTMIP GCM	$\langle\mathscr{F}_{\mathrm{RTMIP\,GCM}}\rangle$, σ (W m^{-2})	1.12, 0.39	–	5.07, 0.43	–	−2.45, 0.35
	$E_{\langle\mathscr{F}_{\mathrm{RTMIP\,GCM}}\rangle}$ (%)	−31.7	–	−7.7	–	−12.5
$\mathrm{MRTA}_{\mathrm{HITRAN92}}$	$\mathscr{F}_{H92}$ (W m^{-2})	1.72	1.78	5.38	−3.59	−2.78
$\mathrm{MRTA}_{\mathrm{HITRAN04}}$	$\mathscr{F}_{H04}$ (W m^{-2})	1.68	1.78	5.33	−3.55	−2.74
$\mathrm{MRTA}_{\mathrm{H92}} - \mathrm{MRTA}_{\mathrm{H04}}$	$\mathscr{F}_{H92} - \mathscr{F}_{H04}$ (W m^{-2})	0.05	0.00	0.05	−0.05	−0.05
AER LBL (a)	$\mathscr{F}_{\mathrm{LBLa}}$ (W m^{-2})	1.74	1.84	5.57	−3.73	−2.85
AER LBL (b)	$\mathscr{F}_{\mathrm{LBLb}}$ (W m^{-2})	1.74	1.84	5.57	−3.73	−2.85
ES `sp_lw_300_orig`	$\mathscr{F}$ (W m^{-2})	1.79	1.90	5.72	−3.82	−2.89
	$\mathscr{F} - \mathscr{F}_{\mathrm{LBLb}}$ (W m^{-2})	0.05	0.05	0.14	−0.09	−0.04
	$E_{\mathscr{F}}$ (%)	2.6	2.9	2.5	2.4	1.6
ES `sp_lw_hadcm3`	$\mathscr{F}$ (W m^{-2})	1.33	1.97	5.62	−3.64	−2.54
	$\mathscr{F} - \mathscr{F}_{\mathrm{LBLb}}$ (W m^{-2})	−0.41	0.13	0.04	0.08	0.31
	$E_{\mathscr{F}}$ (%)	−23.7	6.9	0.8	−2.3	−10.9
ES `sp_lw_hadgem1_1`	$\mathscr{F}$ (W m^{-2})	1.33	1.97	5.62	−3.64	−2.54
	$\mathscr{F} - \mathscr{F}_{\mathrm{LBLb}}$ (W m^{-2})	−0.41	0.13	0.04	0.08	0.31
	$E_{\mathscr{F}}$ (%)	−23.7	6.9	0.8	−2.3	−10.9
ES `sp_lw_hadgem1_3`	$\mathscr{F}$ (W m^{-2})	1.01	1.99	5.61	−3.62	−2.52
	$\mathscr{F} - \mathscr{F}_{\mathrm{LBLb}}$ (W m^{-2})	−0.73	0.14	0.04	0.11	0.33
	$E_{\mathscr{F}}$ (%)	−41.9	7.8	0.7	−2.9	−11.5

arises as errors in upward and downward fluxes are of similar magnitude and opposite signs, yielding an error in the net flux that is unrepresentative of the error in the two streams.

Changes in spectral databases are considered as a possible source of the discrepancy between the Edwards–Slingo code (based on HITRAN 1992, except for water vapour in `sp_lw_hadgem1_3` which uses HITRAN 2001) and the AER LBL code (based on HITRAN 2004). From Table II it is seen that discrepancies between HITRAN 1992 and 2004 in MRTA are at least a factor of two, and in some cases more than an order of magnitude, smaller than the discrepancy between Edwards–Slingo broad-band results and AER LBL. Thus

DOI: 10.1002/qj

differences in the spectral databases are not the major cause of the errors identified here.

Results for the variation of CO_2, CH_4 and N_2O across a wide range of concentrations, using all performance metrics, are given in Figures 1(a), 2(a) and 3(a). For reference, pre-industrial, present, Quaternary minimum and IPCC SRES (Nakićenović *et al.*, 2000) maximum concentrations are shown for each gas. Concentrations outside this range are relevant for millennial climate change and palaeoclimate. In parts (b) and (c) of these figures we show the ranges for which each spectral file yields a flux gradient that is within a specified percentage error, which acts as a summary of the performance of the spectral file.

For CO_2 (Figure 1), the narrow-band code represents changes within the Quaternary and SRES ranges well, with errors in flux gradient generally less than 5% and always within 10%. This would be acceptable for climate change prediction. As this code is used as an internal standard for the suite of Edwards–Slingo codes (Edwards and Slingo, 1996), some improvement at the lower end of the range would be desirable to represent changes during Quaternary glacial cycles. Above 4000 ppmv CO_2, performance of the narrow-band code deteriorates rapidly.

As a group, the performance of the broad-band spectral files considered is very similar, though the most recent, `sp_lw_hadgem1_3`, performs somewhat worse at the surface. At the tropopause, errors within the Quaternary and SRES range approach 20% for individual flux streams; this reduces to 10% for the net flux after the errors of opposite sign partially cancel. At the TOA, the flux gradient agrees well with the LBL code at standard conditions, but deteriorates rapidly to be 35% in error at the maximum of the SRES range, giving a doubling error of $1\,W\,m^{-2}$. At the surface, for standard conditions, the flux gradient error is 22% for `sp_lw_hadcm3` and `sp_lw_hadgem1_1` and 40% for `sp_lw_hadgem1_3`. These deteriorate to 59% and 74% respectively at the maximum of the SRES range. The corresponding doubling errors are 1.6 and $1.9\,W\,m^{-2}$, which are similar to the signal from CO_2 doubling from standard conditions. The correlated-k fits for CO_2 have not been changed between the broad-band spectral files considered, so the differences must arise from overlap with water vapour, which has been updated from HITRAN 1992 to HITRAN 2001 (J. Edwards, personal communication, 2008).

The net forcing at the tropopause determines the response of the model surface temperature to changes in the atmospheric composition (e.g. Figure 7 later). Figure 1(b) indicates that, within most of the SRES and Quaternary range, the broad-band spectral files represent changes in this forcing correctly to within 10% error. Above the SRES maximum, performance declines and errors are over 20%. However, considering the changes in forcing for other levels and streams is a more rigorous test of whether changes to the radiative absorption from changes in gas concentration are properly represented. Figure 1(b) and (c) shows that the errors in these are greater than 20% for the SRES range and above 50% beyond this.

For CH_4 (Figure 2), the narrow-band spectral file gives an error in flux gradient of less than 10% for all fluxes from standard conditions to the maximum of the SRES envelope. At lower pCH_4, typical of Quaternary glacial cycles, the errors at the tropopause approach 20%. Again, performance deteriorates at higher pCH_4.

Each of the broad-band spectral files performs somewhat differently, though in all cases the performance is poor. The flux gradient error for the net flux at the tropopause between pre-industrial and present concentrations is less than 10% for `sp_lw_hadcm3` but is 15%–20% for `sp_lw_hadgem1_1` and `sp_lw_hadgem1_3`. Errors are larger at the surface (for example 38% in `sp_lw_hadgem1_1` and 69% in `sp_lw_hadgem1_3` at pre-industrial conditions) and at the TOA. All the broad-band spectral files erroneously indicate saturation as pCH_4 increases beyond the SRES envelope, `sp_lw_hadcm3` being worst in this regard.

From Figure 2(b), it is seen that `sp_lw_hadcm3` is within 10% error in flux gradient in some streams for much of the SRES range, but neither of the other broad-band spectral files is this accurate. None of the spectral files can represent all fluxes with less than 20% error in flux gradient across the Quaternary and SRES range. It can be noted that as $pCH_4 \ll pCO_2$, the radiative forcing from envisaged anthropogenic changes in CH_4 is relatively small and the climatic consequences of these errors will not be large. This is seen in small doubling errors.

For N_2O (Figure 3), using the metric of flux gradient, all spectral files perform very poorly, including the narrow-band spectral file. For all spectral files, errors in the flux gradient for the net flux at the tropopause are 15%–25% between pre-industrial and present concentrations, with the broad-band spectral files around 30% at the high end of the SRES envelope. Errors are larger at the surface and TOA. In general, the flux gradient is overestimated near present gas concentrations and strongly underestimated at very high gas concentrations. For example, at standard conditions the flux gradient at the surface is overestimated by 60% by `sp_lw_hadgem1_3` and by 80% by `sp_lw_hadcm3` and `sp_lw_hadgem1_1`.

None of the broad-band spectral files represents the changes in the net flux at the tropopause within 20% error for all of the Quaternary and SRES range and none represents changes in all fluxes within 50% error (Figure 3(b) and (c)). As noted for CH_4, present and envisaged N_2O concentrations and radiative forcings are low. The doubling errors within the Quaternary and SRES ranges are typically 5%–10% of the radiative forcing from doubling CO_2.

3.3. Summary

We have used a methodology similar to Collins *et al.* (2006) to compare the long-wave radiative response of the Met Office radiative transfer codes on a fixed profile with results from a line-by-line model. Relative to Collins

DOI: 10.1002/qj

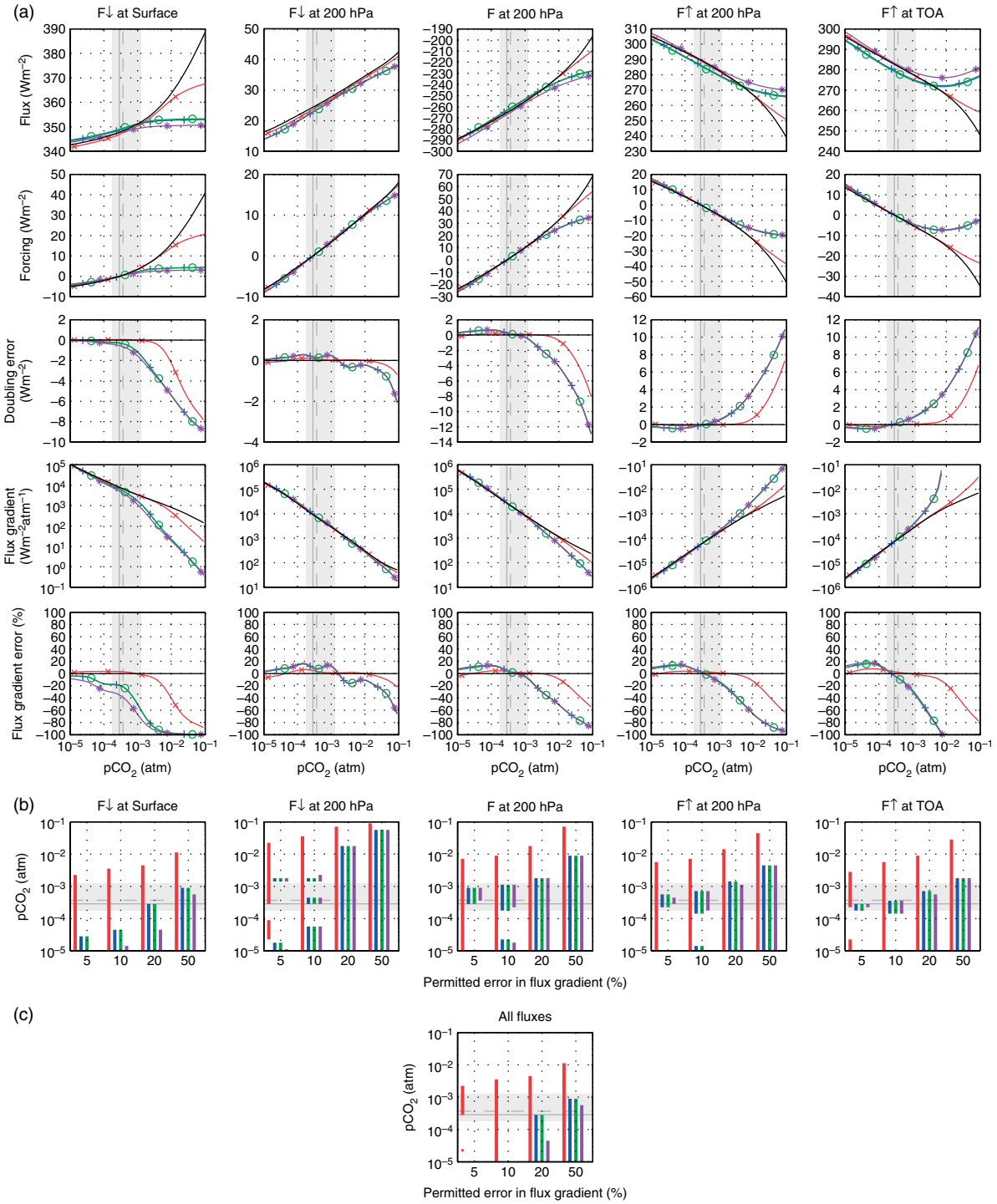

Figure 1. Performance of codes for CO_2. (a) Performance for each level and flux. (b) Region where gas is within specified error for each flux and level. (c) Region where gas is within specified error for all fluxes and levels. Colours (online only) and markers are: black for AER LBL, red × for `sp_lw_300_orig`, blue + for `sp_lw_hadcm3`, green ○ for `sp_lw_hadgem1_1` and purple ∗ for `sp_lw_hadgem1_3`. Order of bars in (b) and (c), from left to right within each group, is: `sp_lw_300_orig`, `sp_lw_hadcm3`, `sp_lw_hadgem1_1`, `sp_lw_hadgem1_3`. Shaded areas indicate the range from Quaternary minimum (180 ppmv) to SRES maximum (1248 ppmv) concentration. Grey lines in these areas are solid for pre-industrial (287 ppmv) and dashed for year 2000 (369 ppmv) concentrations. This figure is available in colour online at www.interscience.wiley.com/journal/qj

et al. (2006), we perform this intercomparison over a wider range of gas concentrations and use a wider variety of metrics to analyse the resulting data. The performance of the broad-band codes used in the UM in calculating changes in the irradiances at the surface and TOA is poor. Performance of the net flux at the tropopause is better, but this is achieved by partial cancellation of opposing errors in upward and downward radiation streams.

For the iconic experiment of CO_2 doubling, performed on a fixed profile, the broad-band ES spectral files do not accurately represent the changes in the radiative flux at

DOI: 10.1002/qj

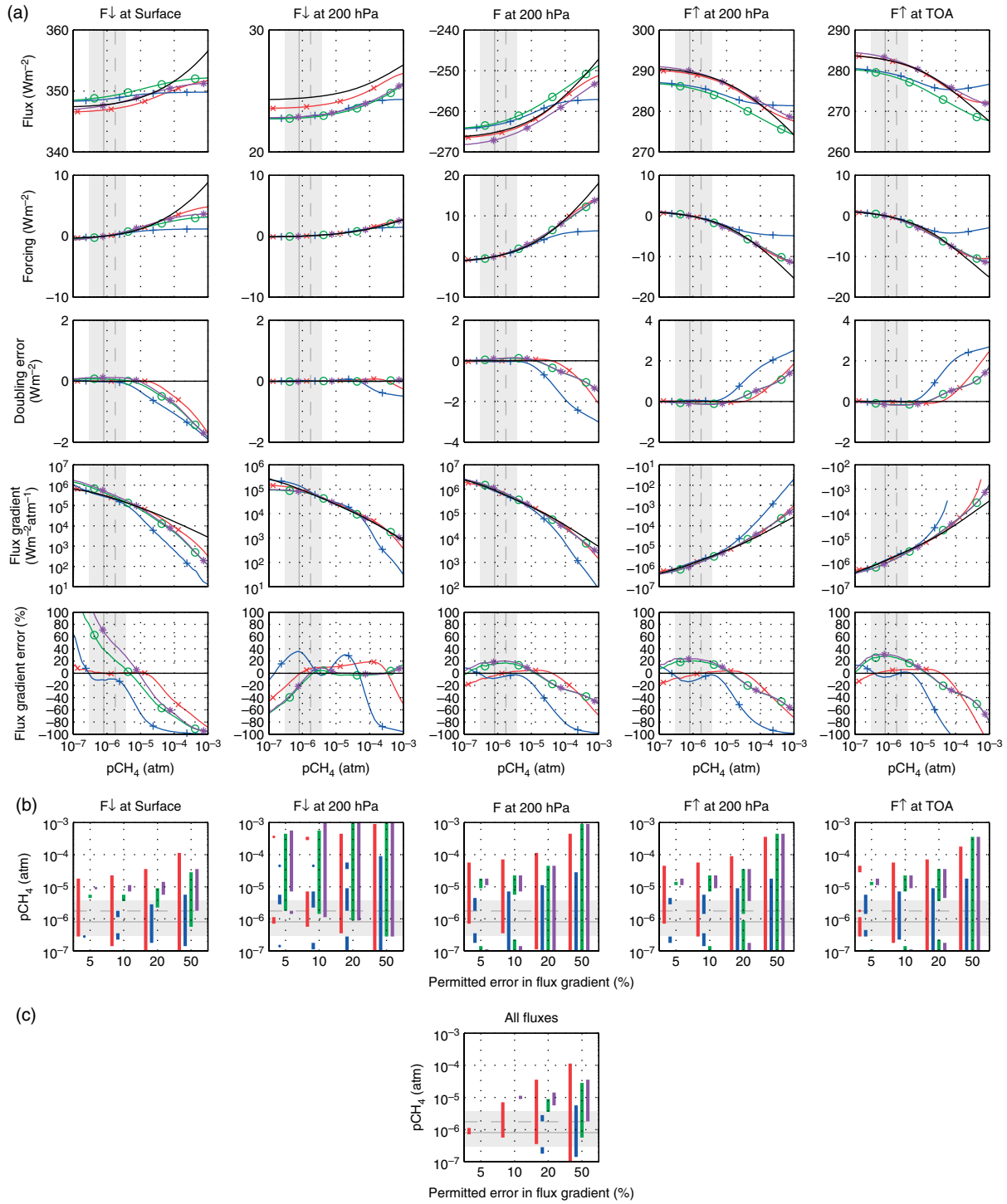

Figure 2. Performance of codes for CH_4. (a) Performance for each level and flux. (b) Region where gas is within specified error for each flux and level. (c) Region where gas is within specified error for all fluxes and levels. Colours (online only) and markers are: black for AER LBL, red × for `sp_lw_300_orig`, blue + for `sp_lw_hadcm3`, green ○ for `sp_lw_hadgem1_1` and purple ∗ for `sp_lw_hadgem1_3`. Order of bars in (b) and (c), from left to right within each group, is: `sp_lw_300_orig`, `sp_lw_hadcm3`, `sp_lw_hadgem1_1`, `sp_lw_hadgem1_3`. Shaded areas indicate the range from Quaternary minimum (300 ppbv) to SRES maximum (3731 ppbv) concentration. Grey lines in these areas are solid for pre-industrial (806 ppbv) and dashed for year 2000 (1760 ppbv) concentrations. This figure is available in colour online at www.interscience.wiley.com/journal/qj

the surface, the TOA or upward and downward fluxes at the tropopause. This is not unusual for radiative transfer codes used in GCMs; Collins *et al.* (2006) show that most radiative transfer codes used in GCMs submitted to IPCC AR4 underestimate long-wave radiative forcing by CO_2.

Comparing different gases, the error in the forcings for CO_2 at the maximum SRES concentration in the ES broad-band codes is of size similar to or larger than the radiative forcings due to CH_4 and N_2O at the SRES maxima.

DOI: 10.1002/qj

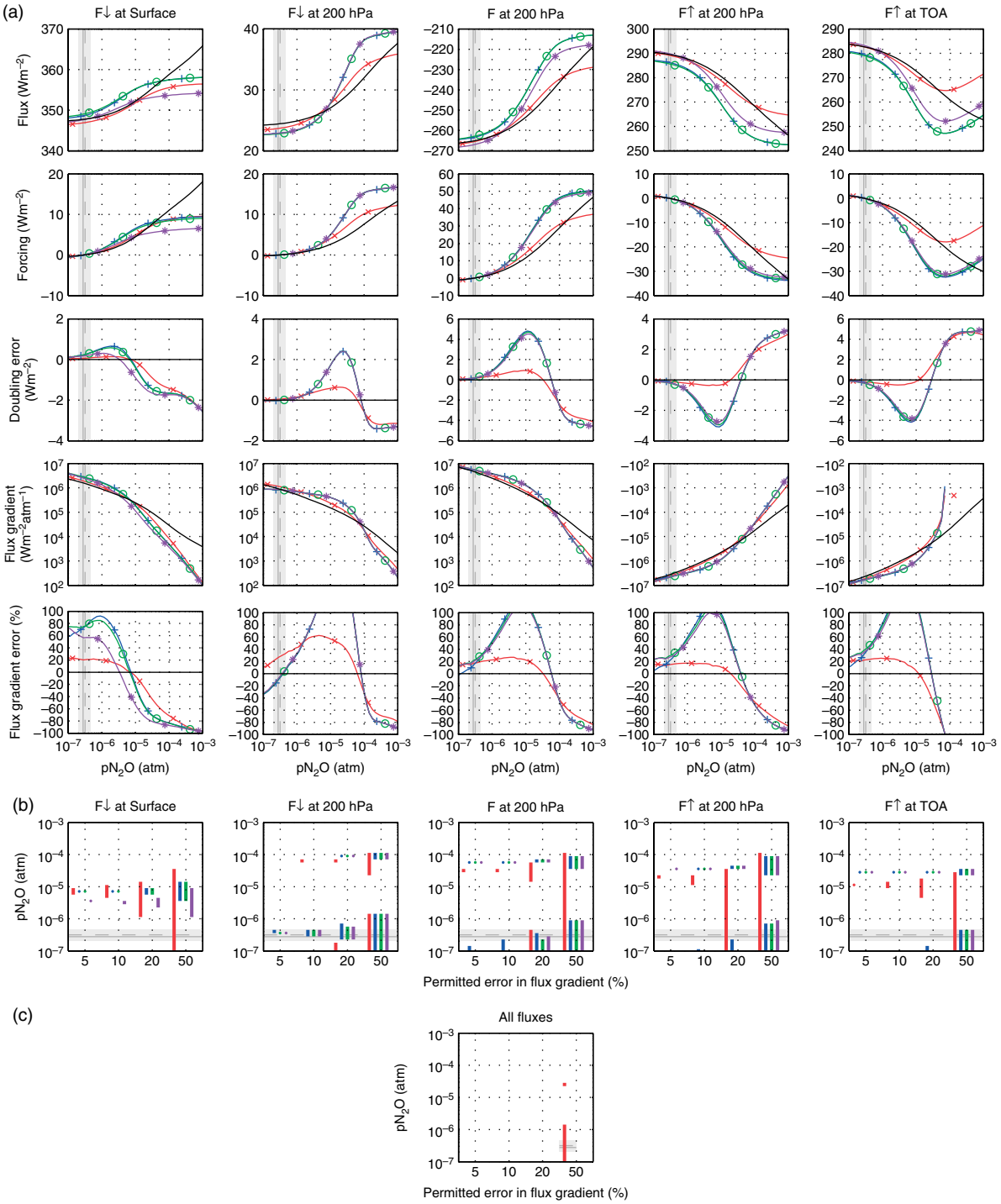

Figure 3. Performance of codes for N_2O. (a) Performance for each level and flux. (b) Region where gas is within specified error for each flux and level. (c) Region where gas is within specified error for all fluxes and levels. Colours (online only) and markers are: black for AER LBL, red × for `sp_lw_300_orig`, blue + for `sp_lw_hadcm3`, green ○ for `sp_lw_hadgem1_1` and purple ∗ for `sp_lw_hadgem1_3`. Order of bars in (b) and (c), from left to right within each group, is: `sp_lw_300_orig`, `sp_lw_hadcm3`, `sp_lw_hadgem1_1`, `sp_lw_hadgem1_3`. Shaded areas indicate the range from Quaternary minimum (200 ppbv) to SRES maximum (460 ppbv) concentration. Grey lines in these areas are solid for pre-industrial (275 ppbv) and dashed for year 2000 (316 ppbv) concentrations. This figure is available in colour online at www.interscience.wiley.com/journal/qj

4. Fixed profile, comparison on full profile

Comparing fluxes at three pressure levels has the benefit of simplicity, but may not give a full picture of the distribution of radiative energy deposition through the atmosphere. We investigate this vertical profiles of fluxes (Figure 4) and radiative heating rates (Figure 5) for increasing CO_2.

The errors in the absolute flux profiles relative to the LBL results for standard conditions ($1 \times CO_2$ in Figures 4 and 5) indicate that the three-level comparison does not fully characterize the profile of flux errors. The errors

DOI: 10.1002/qj

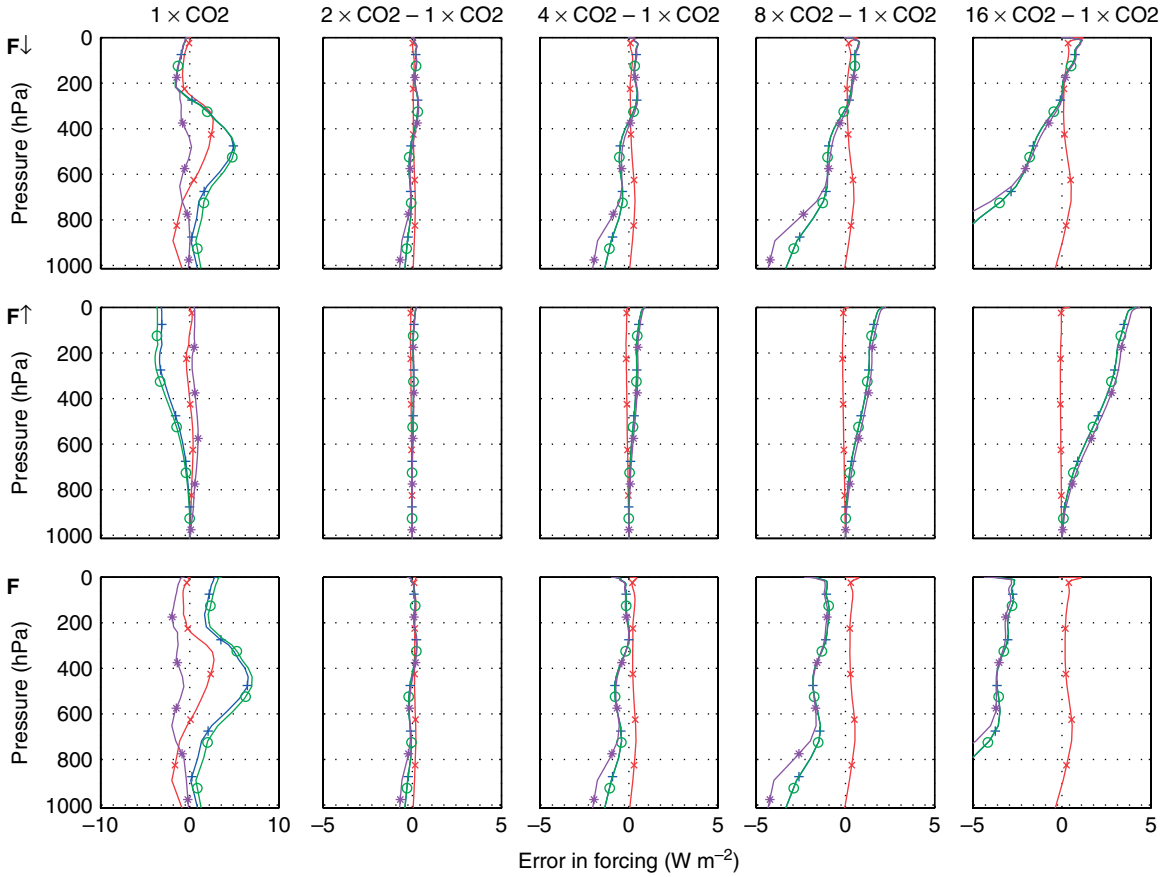

Figure 4. Vertical profile of errors in Edwards–Slingo radiative fluxes relative to AER LBL. Leftmost column is absolute error at $1\times CO_2$; other columns are errors in forcing relative to this. Colours (online only) and markers are: red × for `sp_lw_300_orig`, blue + for `sp_lw_hadcm3`, green ○ for `sp_lw_hadgem1_1` and purple ∗ for `sp_lw_hadgem1_3`. This figure is available in colour online at www.interscience.wiley.com/journal/qj

at the tropopause and surface are significantly smaller than those elsewhere in the atmosphere; the maximum error is 7 W m^{-2} at 450 hPa. One can envisage certain situations, for example an optically thick high-altitude cloud, in which the presence of such errors might perturb the energy balance of the troposphere. In terms of heating, the maximum error at $1 \times CO_2$ is -0.35 W m^{-2}, a large proportion of the typical heating rate of -2 W m^{-2}.

Considering the response across the profile to CO_2 enhancement (Figure 4), the broad-band spectral files give a systematic pattern of errors with height: the error in upward flux becomes larger with height and the error in downward flux becomes smaller with height. This can be understood as there being an insufficient increase in gaseous absorption with increasing CO_2. This is evident at twice pre-industrial CO_2 and this error increases with increasing CO_2. As long-wave fluxes are largest in the lower atmosphere, this is seen most strongly at the surface. Whilst change in the net flux at the tropopause may give a good indication of change in surface temperature (see section 5), the downward flux at the surface or upward flux at the TOA are clearer indicators of whether gaseous absorption is correctly represented.

In radiative heating rate terms, the most notable change with increasing CO_2 is an overestimate of increased heating rate between the surface and 600 hPa by the broad-band spectral files (Figure 5). Extra heating of the troposphere, together with insufficient heating of the surface, may well have the effect of suppressing convection. It is notable that the change in heating rate between $1 \times CO_2$ and $16 \times CO_2$ is of similar size to the absolute error in heating rate from the ES broad-band spectral files at $1 \times CO_2$.

5. Climate model experiments

5.1. Long-wave effect of CO_2

The fixed profile comparisons above consider the effect of changing a single well-mixed radiative absorber. Here, we look at the climatic effect of the errors found in the radiative flux profiles due to changing CO_2. We use the radiative–convective model with a fixed water vapour profile (no water vapour feedback) so that changes in the flux profile are directly attributable to the change in CO_2. As a control, we use the narrow-band spectral files for both long-wave (`sp_lw_300_orig`) and short-wave (`sp_sw_220_orig`) spectral regions. In the comparison runs, we replace the long-wave spectral file with `sp_lw_hadcm3` but use the narrow-band short-wave spectral file (`sp_sw_220_orig`), thus isolating

DOI: 10.1002/qj

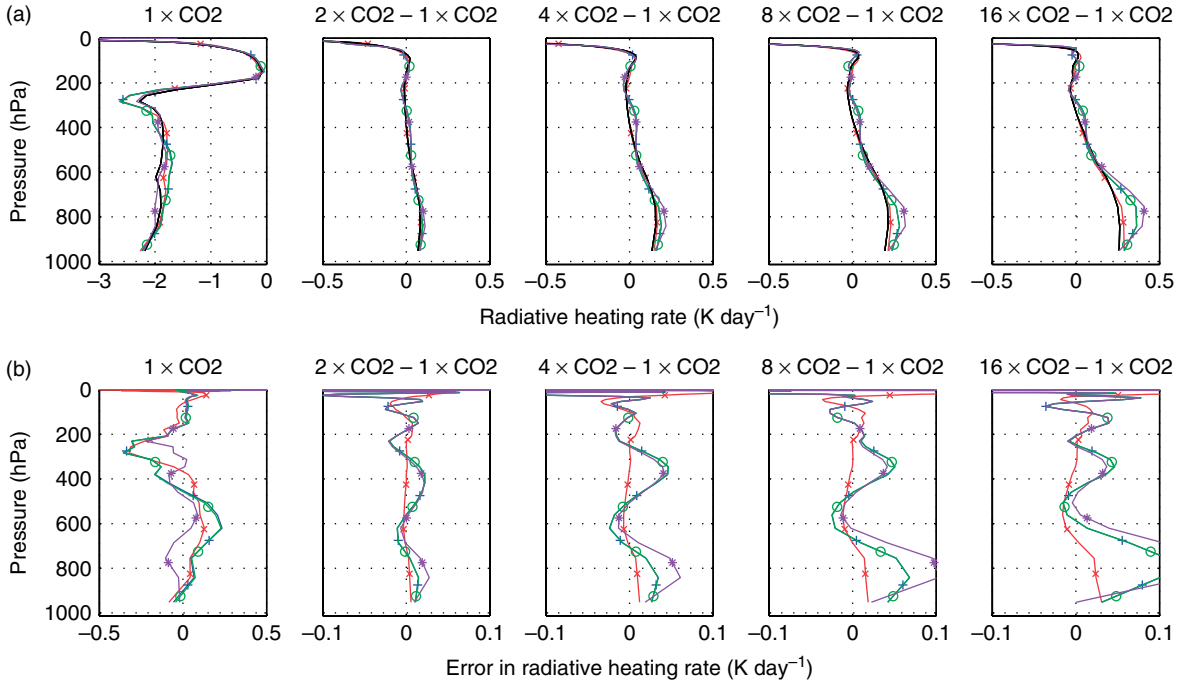

Figure 5. Radiative heating rate. (a) Vertical profiles. (b) Profile of errors relative to AER LBL. Colours (online only) and markers are: black (no marker) for AER LBL, red × for `sp_lw_300_orig`, blue + for `sp_lw_hadcm3`, green ○ for `sp_lw_hadgem1_1` and purple ∗ for `sp_lw_hadgem1_3`. This figure is available in colour online at www.interscience.wiley.com/journal/qj

the long-wave changes. For comparative purposes, we perform a second set of runs with a climatological relative humidity profile (water vapour feedback on). Using a simple climate model is useful to minimize the number of degrees of freedom, thus simplifying the analysis. We would expect GCM responses to be more complex.

Figure 6 shows the surface temperature response to increased CO_2. For the case with no water vapour feedback, it is seen that the change in surface temperature using `sp_lw_hadcm3` is smaller than for the control case. This difference is 0.1 K at four times pre-industrial CO_2, increasing at higher CO_2.

To demonstrate the link between radiative forcings on the fixed profile used above, we plot the change in surface temperature against these (Figure 7). It is seen that the radiative forcing at the tropopause is a good indicator of surface temperature change, as surface temperature shows the same proportionality to this for the cases with and without water vapour feedback.

This result could be taken to indicate that errors in the surface radiative forcing are not important to the performance of a climate model, but this is a somewhat misleading simplification. In Figure 8, we plot the convective flux at the surface of the radiative–convective model. In the control case, the convective flux increases with increasing surface temperature. However, when calculating the long-wave fluxes using `sp_lw_hadcm3`, the convective flux at the surface decreases with increasing surface temperature. This occurs as a result of the major deficit in radiative forcing at the surface, as seen in Figure 1(a). To give the correct surface temperature given the error in the radiative flux profiles, one is relying on dynamical feedback through changed convective fluxes. The change in convection with increased CO_2 and temperature has the wrong sign.

5.2. All absorbers

Using the radiative–convective model with water vapour feedback on, the runs using `sp_lw_hadcm3` show slightly enhanced warming for increases of CO_2 up to eight times pre-industrial, relative to the control run (Figure 6). As discussed, the errors in the representation of CO_2 in `sp_lw_hadcm3` lead to insufficient warming, so this change must be attributed to changes in either specific humidity, q, or temperature.

To investigate this we perform a perturbation experiment, looking at the errors in the HadCM3 spectral files, here both long-wave and short-wave, compared with the narrow-band spectral files. As the standard profile, we use the radiative equilibrium profile for pre-industrial conditions. As the perturbation profile, we use the radiative–convective equilibrium profile for eight times pre-industrial CO_2. We change each of CO_2, q and T, and all combinations of these, from the standard to the perturbation profile. For each spectral file we calculate the change of net radiative flux at the tropopause:

$$\Delta_1 F = F_{\text{perturbed}} - F_{\text{standard}}. \tag{7}$$

We can then calculate the difference between the two spectral files:

$$\Delta_2 F = (\Delta_1 F)_{\text{HadCM3}} - (\Delta_1 F)_{\text{narrow-band}}, \tag{8}$$

which can be considered as the error in HadCM3, relative to the narrow-band internal standard (Figure 9).

DOI: 10.1002/qj

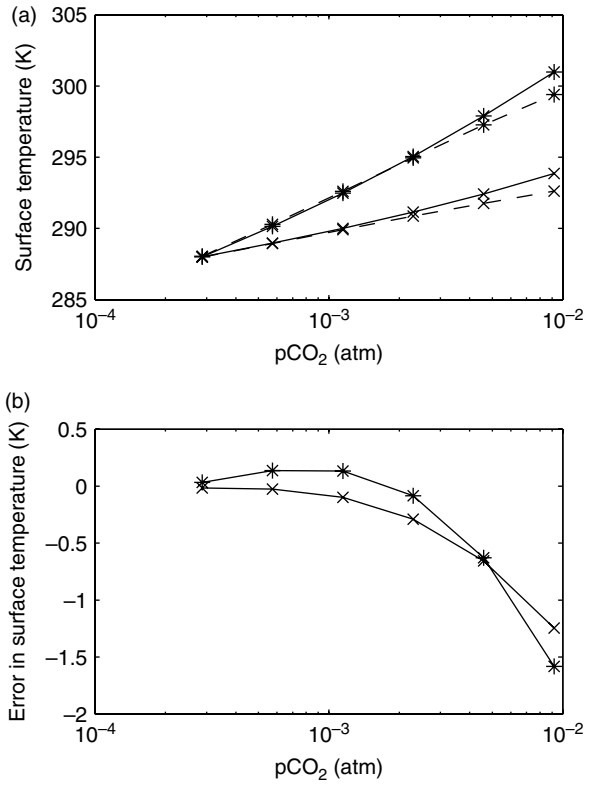

Figure 6. (a) Temperature change with increased CO_2. The solid line is the narrow-band control case, the dashed line uses `sp_lw_hadcm3`. (b) Error in temperature change from `sp_lw_hadcm3` relative to the narrow-band control case. Markers $\times$ and $*$ represent water vapour feedback off and on respectively.

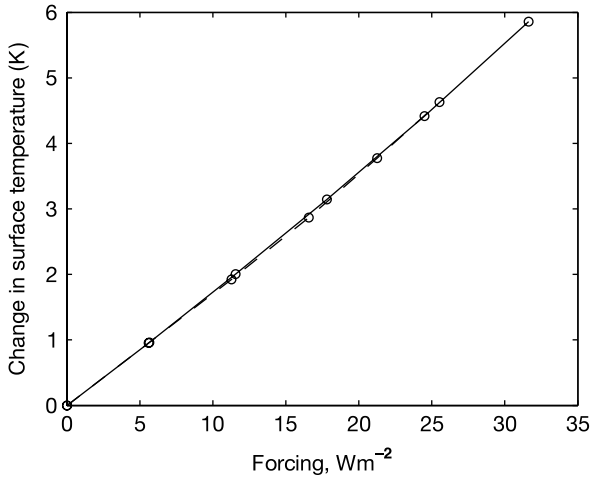

Figure 7. Change in radiative–convective model temperature against radiative forcing on a fixed MLS profile. The solid line is the control case, the dashed line uses `sp_lw_hadcm3`.

In the long-wave, the previously noted underestimation of radiative forcing due to CO_2 is seen. However, the radiative forcing due to increased q is overestimated by a similar amount. In the long-wave, the decrease in flux from increased temperature is overestimated.

In the short-wave, changes in fluxes are much smaller but the errors in HadCM3 are a larger proportion of these. The overall picture is of errors due to each perturbation

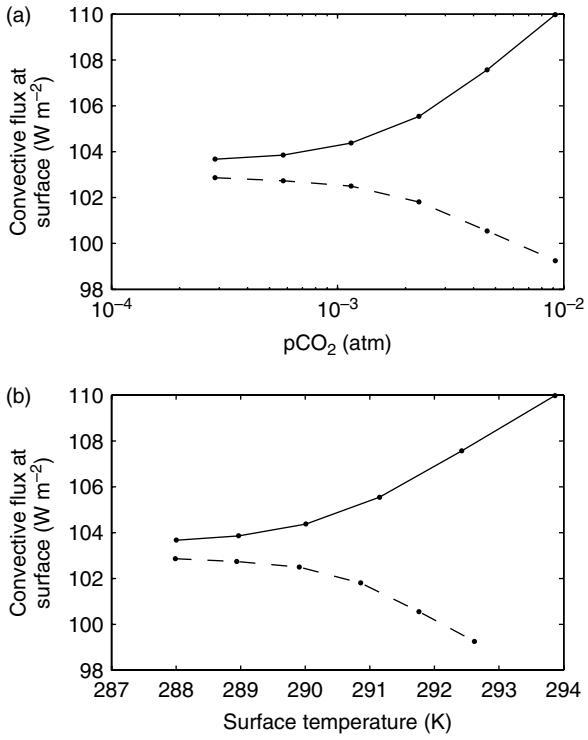

Figure 8. Convective flux with (a) increased CO_2 and (b) corresponding change in temperature. The solid line is the control case, the dashed line uses `sp_lw_hadcm3`.

in both long-wave and short-wave spectral regions. However, the various errors partially cancel such that the overall error is less than many of the constituent errors.

Thus, the initial warming with increased CO_2 seen in the radiative–convective model runs with water vapour feedback on is caused by overestimation of the increasing radiative forcing due to the water vapour increase. Opposing this are an underestimation of the increase in radiative forcing due to increased CO_2 and an overestimation of the decrease in radiative forcing from increased temperature.

Whilst this partial error cancellation occurs for global (temporally and spatially averaged) conditions, it it not certain that it would happen for real conditions. Whilst CO_2 is globally well mixed, variation of water vapour and temperature are of first-order importance. Thus the relative importance of changes in CO_2, q and T will vary globally. It is possible that these errors might lead to a latitudinal error in the change in radiative flux with climate change, but this would need to be the subject of further study.

6. Conclusions

GCMs are a wonderful tool for studying the atmosphere, both for climatic change experiments and process studies, but models are only models and a critical approach to the interpretation of results from them is necessary. In conducting a detailed evaluation of the radiative transfer codes used in recent versions of the Met Office climate model, we have identified some significant shortcomings.

DOI: 10.1002/qj

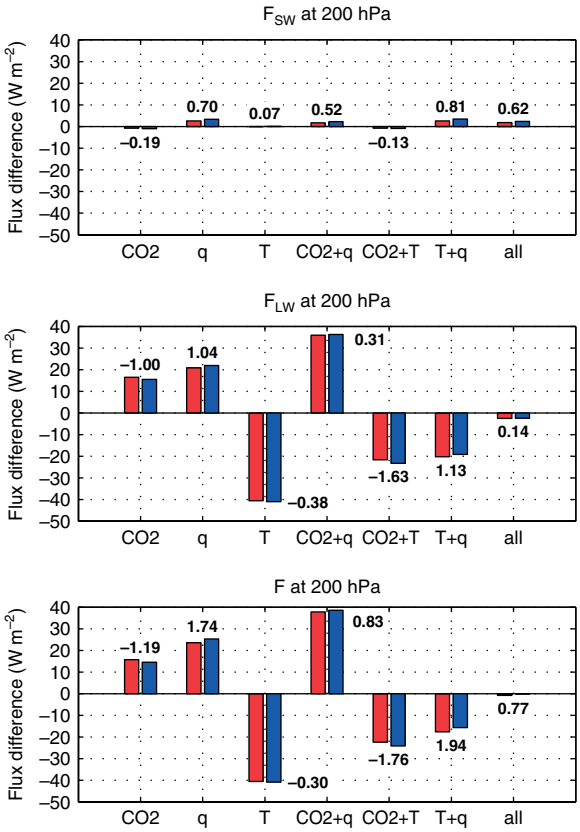

Figure 9. Change in radiative flux from standard to $8 \times CO_2$ profiles ($\Delta_1 F$) for narrow-band (red, left bar) and HadCM3 (blue, right bar) spectral files. The error in HadCM3 relative to the narrow-band ($\Delta_2 F$) is shown in bold text. This figure is available in colour online at www.interscience.wiley.com/journal/qj

For the most important consideration for future climate modelling, increased CO_2, our results for the HadCM3 and HadGEM1 long-wave spectral files can be summarized.

(1) At the tropopause, change in the net flux is represented within 10% error up to around 1000 ppmv. However, upward and downward fluxes have larger errors, which partially cancel.
(2) The changes in the surface and TOA fluxes are significantly underestimated at pre-industrial levels and these errors become much larger at higher CO_2.
(3) Errors consistent with underestimation of increasing gaseous absorption with increasing CO_2 are seen throughout the vertical profile of fluxes.

We investigate the climatic influence of these errors using a radiative–convective model based on the HadCM3 long-wave and short-wave radiative transfer codes, and find the following.

(1) Due to the errors in the vertical distribution of radiative energy, particularly at the surface, the dynamical response to increasing CO_2 is incorrectly represented: the change in convective flux has the wrong sign.
(2) As CO_2 increases, causing an increase in temperature and specific humidity, errors in the change of radiative flux from water vapour partially offset errors in the changes in radiative flux due to CO_2 and temperature.

Discrepancies at the surface may influence other aspects of climate, for example on changes in ocean heat uptake. The errors related to the effect of temperature and water vapour mixing ratio might have consequences for the changes to the meridional energy budget with climatic change, regional energy budgets or for the diurnal cycle. All of these warrant further investigation.

Considering the long-wave effect of other greenhouse gases, the radiative forcing due to changes in CH_4 in the range of Quaternary and SRES concentrations is underestimated by HadCM3 and overestimated by HadGEM1. At higher concentrations that may be of relevance to deeper palaeoclimate (Kiehl and Dickinson, 1987), it is underestimated by all versions of the code. The radiative forcing due to increased N_2O is overestimated in the range of Quaternary and SRES concentrations, but underestimated at very high concentrations.

The performance of the spectral files in our tests can be related to the range of gas concentrations for which they were tuned and the methods used to do this. Thus many aspects of our results can be explained with knowledge of the development of the spectral files, though this is not described in the model documentation (Edwards and Slingo, 1996; Ingram *et al.*, 1997; Cusack *et al.*, 1999; Edwards, 2002, 2003).

In the development of the narrow-band spectral files, maximum column abundances considered were 100kg m^{-2} for CO_2 and 0.1kg m^{-2} for CH_4 and N_2O (J. Edwards, personal communication, 2008). These correspond to mixing ratios of 6.4×10^{-3} for CO_2, 1.8×10^{-5} for CH_4 and 6.4×10^{-6} for N_2O. It is around these values that the strongest deterioration in the performance of the narrow-band spectral file occurs.

In the broad-band spectral files, the cancellation of errors in different streams was engineered into the spectral files in order to reduce the number of k terms needed, so cutting computational cost whilst maintaining a correct net flux at the tropopause. The scientific context a decade ago for this was a strong emphasis on modelling the temperature response to a doubling of CO_2 with limited computational resources. (W. Ingram and J. Edwards, personal communication, 2008). However, this approach has led to poorer representation of fluxes at the surface, the top of the atmosphere and throughout the profile. Furthermore, the recent applications of the code have moved significantly beyond the narrow range of concentrations for which the spectral files were designed (J. Edwards, personal communication, 2008).

Over the last decade, the expectations of the meteorological and wider environmental sciences communities and of policymakers for climate model performance have increased very significantly. The emphasis has widened significantly from prediction of mean surface temperature change to response of all aspects of the climate system to changes in the radiation budget. These changes cannot be suitably modelled if there are large errors in some

DOI: 10.1002/qj

radiative fluxes. Thus we believe that the present scheme, which is heavily tuned to a single flux and relies on cancellation of various errors, warrants revision.

Albeit based on less detailed intercomparisons, we are aware that other broad-band, correlated-k, models perform better than the existing broad-band spectral files for the Edwards–Slingo code (Collins *et al.*, 2006; Goldblatt, 2008), indicating that this is feasible, though some other codes perform worse (Collins *et al.*, 2006). Whether this enhanced performance is at extra computational cost is unknown. However, even if a larger fraction of computational time is required for more accurate radiative transfer calculations, this would be well justified, especially in the context of increased computational resources over the last decade: radiative transfer is at the heart of the climate change problem.

Compared with the methodology used in the intercomparison of radiative transfer codes for IPCC AR4 (Collins *et al.*, 2006), we consider a wider range of gas concentrations and a wider spectral range in long-wave LBL calculations. We also consider upward and downward fluxes separately, examine full vertical profiles of fluxes, use a wider set of metrics to evaluate code/spectral file performance and identify the codes that we compare so that our results may directly inform the interpretation of model results and future model development.

Through analysing our results we have become aware of methodological limitations in our study and others. Our emphasis has been on long-wave fluxes, but errors in short-wave fluxes appear to have similar magnitude to the errors in long-wave fluxes. Following Collins *et al.* (2006), our fixed-profile comparisons were all on a midlatitude summer profile, but errors arise from the overlap between well-mixed greenhouse gases and water vapour, and from temperature changes. We have not considered clouds, but these might affect the cancellation of errors found at the tropopause.

We would make the following suggestions for future intercomparison studies.

(1) Input profiles of altitude, pressure, temperature and gas concentrations should be included in publications to facilitate repeat studies.
(2) Performance of individual models should be identifiable and output profiles of fluxes made available. This would make the intercomparison study more useful, allowing the behaviour of GCMs to be related to the behaviour of the radiative transfer codes that they employ.
(3) Give equal consideration to long-wave and short-wave fluxes.
(4) Consider upward and downward fluxes separately as well as net fluxes.
(5) Consider, as a minimum, the variation in relevant greenhouse gases between Quaternary minimum and SRES maximum concentrations.
(6) Perform intercomparisons for a full range of standard atmospheres (Anderson *et al.*, 1986), from tropical to sub-arctic winter.
(7) Calculate the change in flux with absorber concentration (flux gradient) as an important metric of code performance.
(8) Consider a wider spectral range for LBL calculations to reduce the discrepancy in absolute fluxes.
(9) Consider cloudy skies in addition to clear-sky profiles. The widely used Air Force Geophysical Laboratory standard atmospheres (McClatchey *et al.*, 1971; Anderson *et al.*, 1986), including MLS used here, do not define clouds. Christidis *et al.* (1997) developed a Global Annual Mean atmosphere, which includes clouds and might be a useful starting point in this regard. However, careful consideration would need to be given to the definitions of cloud overlap and other properties (Barker *et al.*, 2003).

For GCM experiments looking at the climate response to changed greenhouse gas concentrations, the accuracy of the radiative transfer code employed underlies all of the model results. Thus the limitations of these codes should be borne in mind when analysing GCM outputs. Specifically, climate models should not be used beyond the range of gas concentrations for which their radiative transfer code was designed and has been shown to be accurate. To improve climate models, we suggest a renewed emphasis on the accuracy of radiative transfer codes.

Acknowledgements

We are grateful to the Met Office for providing us with access to the Edwards–Slingo radiation codes, to Jean-Claude Thelen and James Manners for help with running this and to Atmospheric and Environmental Research Inc. for providing open access to their LBL model. Thanks to John Edwards for extensive discussions regarding the Edwards–Slingo code and for comments on the manuscript. Thanks to James Manners, William Ingram and the late Tony Slingo for discussions regarding the Edwards–Slingo code, to Jim Kasting for initial discussions on model intercomparison in a palaeoclimate context, to Euan Nisbet, Roland von Glasow, Dan Lunt and Paul Valdes for discussions, to Piers Forster and an anonymous reviewer for constructive reviews and to Karen Thurston for comments on the manuscript. CG received funding from NERC through a PhD studentship and the GENIEfy project (NE/C515904/1), from the School of Environmental Science, University of East Anglia, and a NASA Postdoctoral Program fellowship at NASA Ames Research Center, administered by Oak Ridge Associated Universities through a contract with NASA. TML's contribution was part of the NERC Quaternary QUEST (NE/D001676/1) and Feedbacks QUEST (NE/F001657/1) projects.

Appendix

The MLS profile used in this intercomparison is described in Tables AI and AII.

DOI: 10.1002/qj

Table AI. Properties of MLS profile at levels (layer boundaries).

Altitude (km)	Pressure (hPa)	Temperature (K)
70.0	0.067	218.10
69.0	0.078	222.50
67.9	0.091	227.34
66.8	0.107	232.18
65.7	0.126	237.02
64.5	0.149	241.80
63.1	0.179	246.56
61.7	0.216	251.32
60.3	0.261	256.08
58.4	0.334	261.00
56.4	0.431	265.88
53.9	0.589	270.71
47.2	1.339	274.56
44.9	1.782	269.65
42.9	2.292	264.69
40.9	2.964	259.73
38.9	3.853	254.77
36.9	5.035	249.84
34.9	6.613	244.95
32.9	8.786	239.99
30.8	11.801	235.40
29.1	15.069	231.81
27.6	18.791	228.66
26.2	23.156	226.71
24.9	28.120	224.98
23.7	33.733	223.57
22.5	40.535	222.20
21.3	48.690	220.76
20.2	57.694	219.44
19.1	68.429	218.03
18.0	81.200	216.80
16.9	96.490	215.70
15.8	114.564	215.70
14.7	136.511	215.70
13.6	162.913	215.74
12.4	196.440	219.70
11.7	218.668	224.25
11.0	243.000	228.80
10.3	269.015	233.35
9.6	297.469	237.86
8.9	328.507	242.35
8.2	361.862	246.90
7.5	398.085	251.45
6.8	437.556	256.00
6.1	480.526	260.55
5.3	532.986	265.40
4.5	589.841	270.20
3.7	651.552	275.00
2.9	718.704	279.80
2.1	792.287	284.60
1.1	891.460	289.25
0.0	1013.000	294.20

Table AII. Properties of MLS profile in layers.

Pressure (hPa)	Temperature (K)	q (g/g)	fO_3 (ppv)
0.072	220.34	2.34e-06	4.30e-07
0.084	224.97	2.43e-06	4.98e-07
0.099	229.81	2.53e-06	5.80e-07
0.116	234.65	2.62e-06	6.75e-07
0.137	239.61	2.73e-06	7.88e-07
0.164	244.24	2.82e-06	9.02e-07
0.198	249.00	2.93e-06	1.03e-06
0.239	253.76	3.03e-06	1.18e-06
0.298	258.75	3.14e-06	1.36e-06
0.382	263.53	3.22e-06	1.55e-06
0.511	268.77	3.32e-06	1.80e-06
0.963	274.41	3.40e-06	2.82e-06
1.561	272.00	3.40e-06	4.08e-06
2.038	267.05	3.35e-06	5.10e-06
2.628	262.09	3.26e-06	6.30e-06
3.407	257.13	3.17e-06	7.56e-06
4.443	252.17	3.12e-06	8.49e-06
5.825	247.27	3.09e-06	8.83e-06
7.703	242.34	3.05e-06	8.52e-06
10.301	237.51	2.99e-06	7.77e-06
13.419	233.52	2.91e-06	6.96e-06
16.935	230.17	2.82e-06	6.31e-06
20.975	227.61	2.73e-06	5.68e-06
25.640	225.81	2.64e-06	5.03e-06
30.913	224.24	2.52e-06	4.22e-06
37.163	222.88	2.39e-06	3.45e-06
44.591	221.46	2.23e-06	2.83e-06
53.199	220.08	2.12e-06	2.29e-06
63.060	218.72	2.03e-06	1.80e-06
74.819	217.39	1.98e-06	1.25e-06
88.858	216.18	1.98e-06	8.23e-07
105.507	215.70	2.03e-06	6.32e-07
125.467	215.70	2.13e-06	5.24e-07
149.826	215.71	3.00e-06	4.40e-07
179.678	216.81	6.03e-06	3.04e-07
207.590	222.01	1.77e-05	2.28e-07
230.793	226.55	4.07e-05	1.94e-07
255.965	231.10	8.48e-05	1.60e-07
283.268	235.64	1.55e-04	1.31e-07
313.000	240.13	2.28e-04	1.16e-07
345.133	244.65	3.16e-04	1.02e-07
379.985	249.20	4.33e-04	8.92e-08
417.818	253.75	5.95e-04	7.95e-08
458.978	258.30	7.91e-04	6.99e-08
506.779	263.03	1.06e-03	6.13e-08
561.516	267.83	1.49e-03	5.44e-08
620.757	272.63	2.26e-03	4.89e-08
685.061	277.43	3.28e-03	4.39e-08
755.392	282.23	4.77e-03	3.95e-08
841.897	287.03	6.98e-03	3.55e-08
952.115	291.77	9.92e-03	3.19e-08

DOI: 10.1002/qj

References

Anderson GP, Clough SA, Kneizys FX, Chetwynd JH, Shettle EP. 1986. AFGL atmospheric constituent profiles (0–120 km). *Environmental Research Papers 954*. Air Force Geophysical Laboratory: Hanscom AFB, MA.

Barker HW, Stephens GL, Partain PT, Bergman JW, Bonnel B, Campana K, Clothiaux EE, Clough S, Cusack S, Delamere J, Edwards J, Evans KF, Fouquart Y, Freidenreich S, Galin V, Hou Y, Kato S, Li J, Mlawer E, Morcrette J, O'Hirok W, Risnen P, Ramaswamy V, Ritter B, Rozanov E, Schlesinger M, Shibata K, Sporyshev P, Sun Z, Wendisch M, Wood N, Yang F. 2003. Assessing 1D atmospheric solar radiative transfer models: Interpretation and handling of unresolved clouds. *J. Climate* **16**: 2676–2699.

Bergman NM, Lenton TM, Watson AJ. 2004. COPSE: a new model of biogeochemical cycling over the Phanerozoic. *Am. J. Sci.* **304**: 397–437.

Christidis N, Hurley MD, Pinnock S, Shine KP, Wallington TJ. 1997. Radiative forcing of climate change by CFC-11 and possible CFC replacements. *J. Geophys. Res.* **102**: 19597–19609.

Clough SA, Iacono MJ. 1995. Line-by-line calculation of atmospheric fluxes and cooling rates – 2. Application to carbon dioxide, ozone, methane, nitrous oxide and the halocarbons. *J. Geophys. Res.* **100**: 16 519–16 535.

Clough SA, Iacono MJ, Moncet JL. 1992. Line-by-line calculations of atmospheric fluxes and cooling rates: application to water vapor. *J. Geophys. Res.* **97**: 15 761–15 785.

Clough SA, Shephard MW, Mlawer EJ, Delamere JS, Iacono MJ, Cady-Pereira K, Boukabara S, Brown PD. 2005. Atmospheric radiative transfer modeling: A summary of the AER codes. *J. Quant. Spectrosc. Radiat. Transfer* **91**: 233–244.

Collins WD, Ramaswamy V, Schwarzkopf MD, Sun Y, Portmann RW, Fu Q, Casanova SEB, Dufresne JL, Fillmore DW, Forster PMD, Galin VY, Gohar LK, Ingram WJ, Kratz DP, Lefebvre M, Li J, Marquet P, Oinas V, Tsushima Y, Uchiyama T, Zhong WY. 2006. Radiative forcing by well-mixed greenhouse gases: Estimates from climate models in the Intergovernmental Panel on Climate Change (IPCC) Fourth Assessment Report (AR4). *J. Geophys. Res.* **111**: D14 317.DOI:10.1029/2005JD006713.

Cusack S, Edwards JM, Crowther JM. 1999. Investigating *k* distribution methods for parameterizing gaseous absorption in the Hadley Centre Climate Model. *J. Geophys. Res.* **104**: 2051–2057.

Edwards JM. 2002. *A short user's guide to the radiation code (version with preprocessing)*. Technical report. The Met Office: Bracknell, UK.

Edwards JM. 2003. *Interim documentation for the Radience Code in F90*. Technical report. The Met Office: Bracknell, UK.

Edwards JM, Slingo A. 1996. Studies with a flexible new radiation code. I: Choosing a configuration for a large scale model. *Q. J. R. Meteorol. Soc.* **122**: 689–719.

Ellingson RG, Ellis J, Fels S. 1991. The intercomparison of radiation codes used in climate models: long wave results. *J. Geophys. Res.* **96**: 8929–8953.

Goldblatt C. 2008. *Bistability of atmospheric oxygen, the Great Oxidation and climate*. PhD thesis: Univ. East Anglia.

Goody RM, Yung YL. 1989. *Atmospheric Radiation*. Oxford University Press: Oxford, UK. 2nd edn.

Ingram WJ, Woodward S, Edwards JM. 1997. Radiation. *Unified Model Documentation Paper 23*. Meteorological Office: Bracknell, UK.

Kasting JF, Pollack JB, Crisp D. 1984. Effects of high CO_2 levels on surface temperature and atmospheric oxidation-state of the early Earth. *J. Atmos. Chem.* **1**: 403–428.

Kiehl JT, Dickinson RE. 1987. A study of the radiative effects of enhanced atmospheric CO_2 and CH_4 on early Earth surface temperatures. *J. Geophys. Res.* **92**: 2991–2998.

Kratz DP. 2008. The sensitivity of radiative transfer calculations to the changes in the hitran database from 1982 to 2004. *J. Quant. Spectrosc. Radiat. Transfer* **109**:1060–1080. DOI: 10.1016/j.jqsrt.2007.10.010.

Lenton TM. 2006. Climate change to the end of the millennium. *Climatic Change* **76**: 7–29.

Lenton TM, Williamson MS, Edwards NR, Marsh R, Price AR, Ridgwell AJ, Shepherd JG, Cox SJ. 2006. Millennial timescale carbon cycle and climate change in an efficient Earth system model. *Clim. Dyn.* **26**: 687–711.

Manabe S, Wetherald RD. 1967. Thermal equilibrium of the atmosphere with a given distribution of relative humidity. *J. Atmos. Sci.* **24**: 241–259.

McClatchey RA, Fenn RW, Selby JEA, Volz FE, Garling JS. 1971. Optical properties of the atmosphere (revised). *Environmental Research Papers 354*. Air Force Cambridge Research Laboratories: Cambridge, UK.

Nakićenović N, Alcamo J, Davis G, de Vries B, Fenhann J, Gaffin S, Gregory K, Grübler A, Jung TY, Kram T, La Rovere EL, Michaelis L, Mori S, Morita T, Pepper W, Pitcher H, Price L, Riahi K, Roehrl A, Rogner HH, Sankovski A, Schlesinger M, Shukla P, Smith S, Wart R, van Rooijen S, Victor N, Dadi Z. 2000. *IPCC Special Report on Emissions Scenarios*. Cambridge University Press: Cambridge, UK.

Pope V, Brown S, Clark R, Collins M, Collins W, Dearden C, Gunson J, Harris G, Jones C, Keen A, Lowe J, Ringer M, Senior C, Sitch S, Webb M, Woodward S. 2007. The Met Office Hadley Centre climate modelling capability: The competing requirements for improved resolution, complexity and dealing with uncertainty. *Philos. Trans. R. Soc. London* **365**: 2635–2657.

Rothman LS, Gamache RR, Tipping RH, Rinsland CP, Smith MAH, Benner DC, Devi VM, Flaud J, Camy-Peyret C, Perrin A, Goldman A, Massie ST, Brown LR, Toth RA. 1992. The HITRAN molecular database: Editions of 1991 and 1992. *J. Quant. Spectrosc. Radiat. Transfer* **48**: 469–507.

Rothman LS, Barbe A, Benner DC, Brown LR, Camy-Peyret C, Carleer MR, Chance K, Clerbaux C, Dana V, Devi VM, Fayt A, Flaud J, Gamache RR, Goldman A, Jacquemart D, Jucks KW, Lafferty WJ, Mandin J, Massie ST, Nemtchinov V, Newnham DA, Perrin A, Rinsland CP, Schroeder J, Smith KM, Smith MAH, Tang K, Toth RA, Vander Auwera J, Varanasi P, Yoshino K. 2003. The HITRAN molecular spectroscopic database: Edition of 2000 including updates through 2001. *J. Quant. Spectrosc. Radiat. Transfer* **82**: 5–44.

Rothman DH, Jacquemart D, Barbe A, Chris Benner D, Birk M, Brown LR, Carleer MR, Chackerian CJ, Chance K, Coudert LH, Dana V, Devi VM, Flaud JM, Gamache RR, Goldbman A, Hartmann JM, Jucks KW, Maki AG, Mandin JY, Massie ST, Orphal J, Perrin A, Rinsland CP, Smith MAH, Tennyson J, Tolchenov RN, Toth RA, Vander Auwera J, Varanasi P, Wager G. 2005. The HITRAN 2004 molecular spectroscopic database. *J. Quant. Spectrosc. Radiat. Transfer* **96**: 139–204.